ELSEVIER

Journal of Neuroscience Methods 159 (2007) 116–124

JOURNAL OF NEUROSCIENCE METHODS

www.elsevier.com/locate/jneumeth

Flexible multielectrodes can resolve multiple muscles in an insect appendage

Andrew J. Spence [a,*], Keith B. Neeves [b], Devon Murphy [c], Simon Sponberg [a], Bruce R. Land [d], Ronald R. Hoy [d], Michael S. Isaacson [e]

[a] *Department of Integrative Biology, University of California at Berkeley, Berkeley, CA 94720, USA*
[b] *School of Chemical and Biomolecular Engineering, Cornell University, Ithaca, NY 14850, USA*
[c] *Pacific Biosciences, Menlo Park, CA, USA*
[d] *Department of Neurobiology and Behavior, Cornell University, Ithaca, NY 14850, USA*
[e] *Baskin School of Engineering, University of California at Santa Cruz, Santa Cruz, CA, USA*

Received 16 May 2006; received in revised form 6 July 2006; accepted 6 July 2006

Abstract

Research into the neuromechanical basis of behavior, either in biomechanics, neuroethology, or neuroscience, is frequently limited by methods of data collection. Two of the most pressing needs are for methods with which to (1) record from multiple neurons or muscles simultaneously and (2) perform this recording in intact, behaving animals. In this paper we present the fabrication and testing of flexible multielectrode arrays (fMEAs) that move us significantly towards these goals. The fMEAs were used to record the activity of several distinct units in the coxa of the cockroach *Blaberus discoidalis*. The devices fabricated here address the first goal in two ways: (1) their flexibility allows them to be inserted into an animal and guided through internal tissues in order to access distinct groups of neurons and muscles and (2) their recording site geometry has been tuned to suit the anatomy under study, yielding multichannel spike waveforms that are easily separable under conditions of spike overlap. The flexible nature of the devices simultaneously addresses the second goal, in that it is less likely to interfere with the natural movement of the animal.

Keywords: Flexible multielectrode arrays; Electromyography; Electrophysiology; Biomechanics; Polyimide; Parylene; Microfabrication; Insects; Arthropods; Cockroach; *Blaberus discoidalis*

1. Introduction

Understanding how groups of neurons and muscles work to take in sensory information, perform computation, and produce behavior is a central challenge of modern science. While studies of parts of arthropod nervous systems (Bassler and Buschges, 1998; Frye and Olberg, 1995; Marder and Calabrese, 1996; Theunissen et al., 1996), reflex pathways (Bassler, 1993; Gronenberg, 1995a,b; Pearson et al., 1976), kinematics (Mu and Ritzmann, 2005), and musculoskeletal systems (Ahn and Full, 2002; Quimby et al., 2006) have produced a wealth of information, it has become increasingly apparent that understanding how even "simple" organisms behave at the systems level requires an integrated picture of the neural and musculoskeletal systems (Full and Koditschek, 1999; Koditschek et al., 2004). This requires new theoretical and experimental tools. Theoretical and mathematical models of the function of neural circuitry (Durr et al., 2004; Ghigliazza and Holmes, 2004; Weimann et al., 1997), the musculoskeletal system (Ghigliazza and Holmes, 2005; Winters and Woo, 1990), and locomotion (Ghigliazza et al., 2003; Seipel et al., 2004) are becoming increasingly sophisticated. For instance, Holmes et al. (2006) have formulated a mathematical model of hexapod locomotion that extends from ion-channel currents to center-of-mass dynamics, by way of model neurons, a simple central pattern generator network, and 6 two-component legs with Hill-type muscle actuation. These mathematical frameworks are beginning to incorporate reasonably realistic physiological details of many components of the organism. As a result, a flurry of hypotheses about how the organism behaves as an integrated system are being formulated. Obtaining experimental data to confirm or refute these new hypotheses is difficult, however. Verification or refutation

* Corresponding author at: Poly-PEDAL Laboratory, Department of Integrative Biology, 3060 Valley Life Sciences Building #3140, University of California at Berkeley, Berkeley, CA 94720-3140, USA. Tel.: +1 510 847 9816.
E-mail address: aspence@nature.berkeley.edu (A.J. Spence).

0165-0270/$ – see front matter © 2006 Elsevier B.V. All rights reserved.
doi:10.1016/j.jneumeth.2006.07.002

of these more complex, systems level models requires (a) the observation and dynamic manipulation of many variables simultaneously, such as the activity of multiple neurons and muscles, sense organs, kinematic data, and forces and (b) the measurements need be performed on intact, behaving organisms.

For vertebrates, implanted wire electromyographic (EMG) techniques (Deliagina et al., 2000; Gregor et al., 2006; Higham and Jayne, 2004) and neurophysiological techniques such as multi-wire (Leutgeb et al., 2005), and silicon multielectrode arrays (Lehmkuhle et al., 2006 and Cyberkinetics, Foxboro, MA) have yielded important multi-unit data in animal preparations that range from fully restrained to freely behaving. For studies encompassing the neuromuscular system, however, invertebrates present appealing model systems as the central nervous system, innervation, and activation of muscles by motoneurons are typically much simpler. The small size of invertebrates has made finding techniques and fabricating devices for multiunit recording more difficult, however. While electromyography of multiple units has been achieved in freely behaving arthropods using multiple wire bipolar recordings with tethered (Mu and Ritzmann, 2005) and even multichannel radiofrequency telemetric (Ando et al., 2002; Kutsch, 2002; Takeuchi and Shimoyama, 2004) preparations, the problems inherent with puncturing the cuticle in multiple places and shepherding multiple wires around moving appendages frequently limit these techniques. The device we present can resolve multiple muscles in a single appendage, requires only a single cuticular incision and bundles all external conductors into a single flexible strip.

Flexible microfabricated devices are increasingly being used to interface with biological tissues. Polymer fabrication techniques have been employed to create flexible MEAs (fMEAs) for retinal prostheses (Margalit et al., 2002; Rodger et al., 2005), studies of the vertebrate retina (Smirnakis et al., 1997), surface EMGs from human subjects (Lapatki et al., 2004), and recording and stimulation of peripheral nerves (Rodriguez et al., 2000; Stieglitz and Gross, 2002). While rigid MEAs fabricated from silicon or glass have found success as substrates for cell culture (Berdondini et al., 2006; James et al., 2004) and where penetration of tissue is required (see Christensen et al. (2000) and Wise (2005), and extensive work by the Center for Neural Communication Technology at the University of Michigan), flexible arrays offer advantages in cuff applications (Stieglitz et al., 2003) where they can be bent around a nerve, or, as we show here, they can be inserted into smaller arthropod appendages in a manner that accesses several muscles simultaneously.

In this article we present flexible multielectrode arrays (fMEAs) and accompanying interface instrumentation that can resolve several distinct neuromuscular units in an arthropod appendage, with strong isolation of spikes to individual channels or small subsets of the array. Their flexible nature allows them to bend around the inside of an insect appendage, accessing distinct muscle groups, while preliminary high speed videography of animals running with an implanted sham electrode suggests that the inserted device does not affect the kinematics of the animal's locomotion. These results suggest that fMEAs may enable multiunit recording from distributed parts of the neuromuscular systems of behaving insects.

We used polyimide as a substrate with which to fabricate our first generation fMEAs. With these devices we found that flexible MEAs could be successfully inserted and used to gather multi-unit data from our cockroach preparation. Their recording site geometry was not optimized for the morphology of the animal, however. In our second generation devices, we realigned the recording sites to match the anatomy, and utilized parylene as a substrate for the fMEAs. Alignment of the recording sites to anatomy yielded vastly improved isolation of units, and the devices made from parylene C, whose electrical and mechanical properties are very similar to polyimide, were the product of a simpler and more rapid fabrication process. Parylene C is increasingly being used for electrophysiological devices, having pinhole-free conformality and low water permeability when compared with polyimide (Rodger et al., 2005).

Working with and testing multielectrode arrays commonly requires expensive or bulky interfacing technologies and amplification electronics. We therefore present a compact 16 channel interconnection device and accompanying multichannel extracellular amplifier.

2. Methods

2.1. Polymer multielectrode microfabrication

A schematic of the polymer multielectrode fabrication process is seen in Fig. 1D, with the completed devices shown in Fig. 1A and B. Flexible polyimide multielectrodes were fabricated at the Cornell Nanofabrication Facility (Murphy, 2003). Devices consisted of a single metallization layer sandwiched between insulating layers of polyimide. A three mask photolithographic process was used to pattern the layers of polyimide and metal into working planar structures. A 500 nm layer of sacrificial silicon dioxide was deposited on 4-in. bare silicon wafers using plasma enhanced chemical vapor deposition (PECVD). The first layer of polyimide (PWDC-1000 Photoneece, Toray Industries and Dow Corning) was then spin-coated on the surface to a thickness of 10 μm. This layer of polyimide was exposed and developed using standard photolithographic techniques to define the base of the multielectrode structure. The base polyimide layer was then fully cured to a thickness of 7 μm. The use of photosensitive polyimide (PWDC-1000 Photoneece) greatly simplifies the fabrication process, as it can simply be spun-on, exposed, developed and cured to produce the final patterned layer. Patterning non-photosensitive polyimide typically requires a lengthy oxygen plasma etch with a metal or thick photoresist mask.

Wafers were then spin-coated with 1.8 μm of photoresist (Shipley S1818) and an image reversal carried out to reverse the tone of the photoresist (Fig. 1D). This resist layer defines the shape of the gold electrode traces that will be evaporated onto the wafer, with the image reversal used to create a negatively sloped resist profile appropriate for metal liftoff. Electron beam evaporation is then used to deposit 15 nm of titanium and 250 nm of gold. The wafer is placed in an ultrasonic portable bath filled with acetone until the resist has lifted the metal off of the wafer everywhere except on electrode array traces. Following this, the

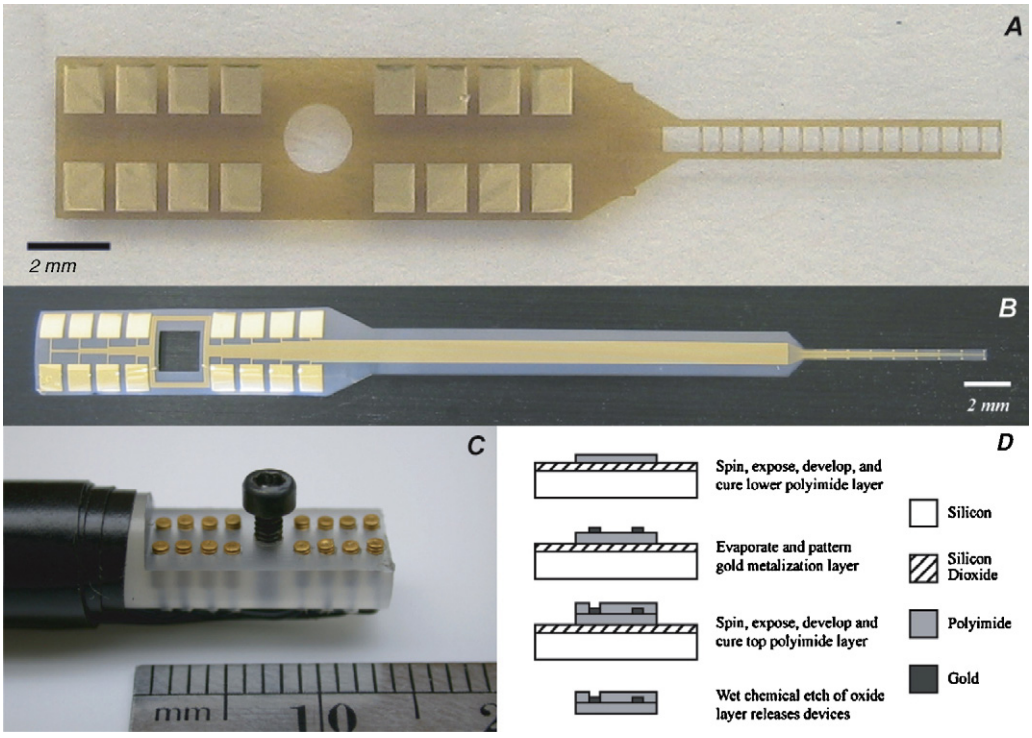

Fig. 1. Flexible multi-electrode arrays (fMEAs, A and B), their fabrication process (D) and miniature bellows interconnect (C). Completed polyimide (A) and parylene (B) fMEAs. The large rectangular gold interconnect pads at the base of the fMEAs (A and B, left) are bolted face down onto the corresponding gold bellows contacts of the interconnect (C). The geometries of the recording sites along the fMEA shanks (A and B, right) are illustrated in Figs. 4 and 6. See Section 2.1 of text for details of the fabrication process in (D).

second polyimide layer is spun, patterned, and cured to 2 μm thickness, encapsulating the electrode wires while exposing the tissue-electrode and electrode-interconnect interfaces. The final step of the process is a wet chemical etch of the sacrificial oxide layer in buffered oxide etch solution (BOE 6:1; 6 parts 40% NH_4F to 1 part 49% HF) to release the probes from the silicon substrate.

Parylene devices were fabricated with a fabrication process similar to that of polyimide devices. Briefly, 5.5 μm of Parylene C were deposited (Specialty Coating Systems PDS-2010) on clean 100 mm wafers. The surface of the parylene was roughened before the lift-off procedure to enhance adhesion with metal layers. The lift-off procedure was identical to polyimide devices. A 1 μm insulating layer of parylene was deposited following metal deposition and patterning. The recording and bonding pads were defined by selectively etching the insulating parylene layer using a photoresist mask and an oxygen plasma. Finally, the device geometry was defined by a second oxygen plasma etch, again using a photoresist mask. Once the final etch is complete, devices are peeled off the wafer and ready for use. There is no need for a lengthy oxide etch to release the Parylene devices, as with the polyimide devices, however the two substrates have similar mechanical and electrical properties (Table 1) and biocompatibility.

The impedance the fMEA recording sites was measured against a silver–silver chloride ground in saline ringer solution. Recording sites on the polyimide array had an impedance of $32 \pm 3.8\,k\Omega$ ($n = 10$) at 800 Hz, while those of the parylene array had an impedance of $38 \pm 0.3\,k\Omega$ ($n = 3$) at 800 Hz.

2.2. Interconnect fabrication

The multielectrode interconnect (Fig. 1C) was fabricated from 6.4 mm ((1/4)-in.) diameter KEL-F rod (McMaster-Carr) and miniature gold plated bellows contact springs (Servometer, part number 2510). A 13 mm × 5 mm flat was milled on one end of the rod, and an M1.6 threaded hole tapped through in the center of this flat. Two rows of eight holes, 1 mm in diameter, were milled 1.7 mm deep into the flat surface, followed by a 0.5 mm diameter hole the rest of the way through the rod in the center of each 1 mm hole. The gold contact springs sit in the larger holes, with their convoluted spring contact projecting above the surface by 0.3 mm, which is their maximum compression distance. Fine hook-up wire (30 AWG, Digikey Inc.) was soldered to the base of the spring contact and fed through the 0.5 mm hole as the contact was placed in the larger diameter hole.

Table 1
Mechanical and electrical properties of polyimide and parylene

Property	Polyimide (PWDC-1000)	Parylene C
Tensile strength (MPa)	130	70
Young's modulus (GPa)	3.0	2.8
Dielectric constant	2.9	3.1
Volume resistivity (Ω cm)	$>10^{16}$	8.8×10^{16}
Surface resistivity (Ω)	$>10^{16}$	10^{14}

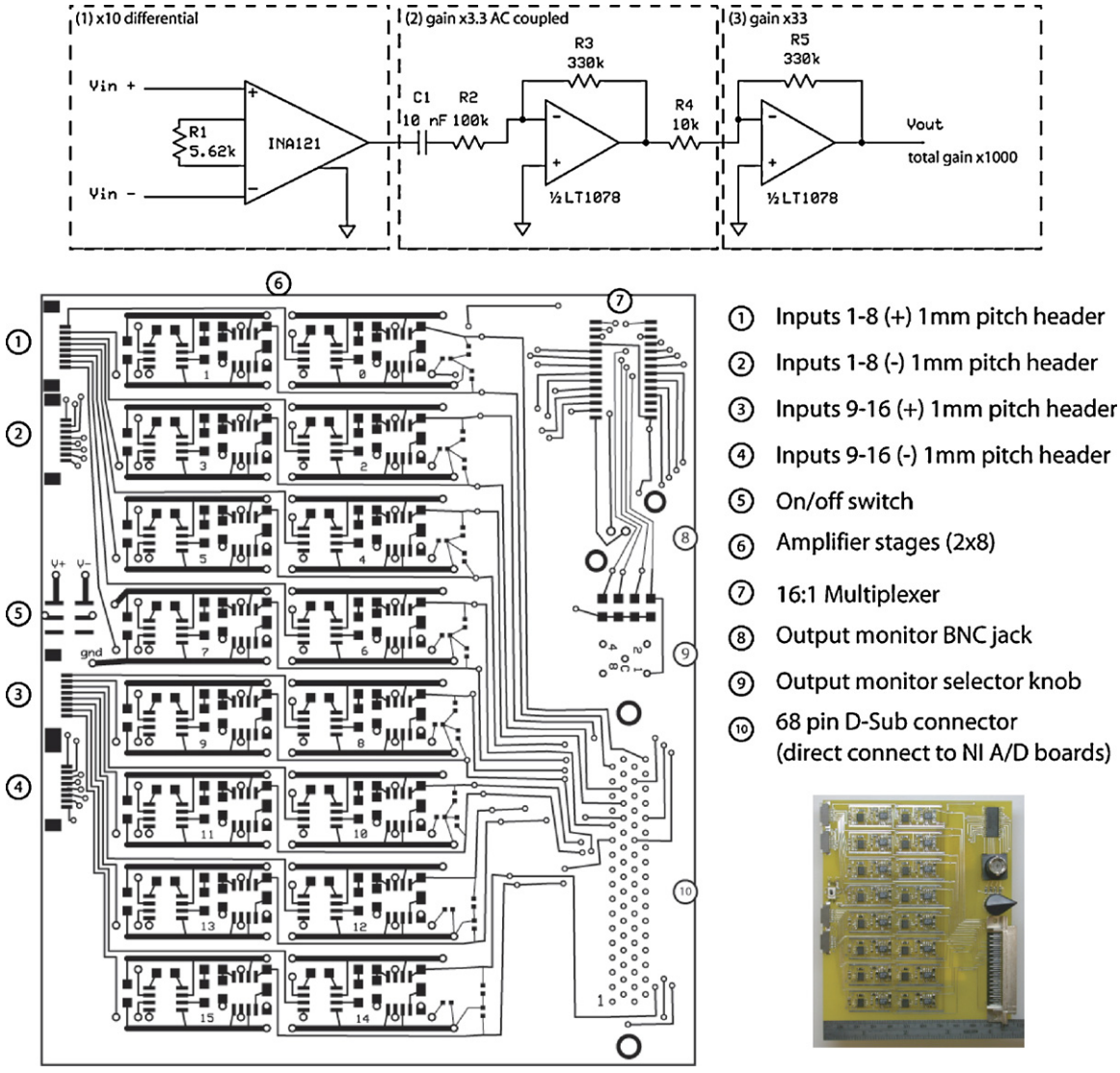

Fig. 2. Multichannel extracellular amplifier. Block diagram of an individual channel (top), top surface of the printed circuit board layout (middle), and photo of completed amplifier (bottom right). The completed 16 channel amplifier measures 4.5 in. × 5 in. × 3 in.

2.3. Amplifier design and fabrication

The multichannel extracellular amplifier was built from low-power, high precision surface mount components, soldered to a printed circuit board (Fig. 2). The board was designed using freely available layout software (www.expresspcb.com), and the use of surface mount components resulted in a small footprint of 4.5 in. × 5 in., for the entire 16 channel amplifier. The design parameters for the amplifier required it to be a high input impedance, ac coupled, differential voltage amplifier with a gain of ∼1000 and a bandwidth of at least 5 kHz. This goal was realized using the three op-amp circuit seen in Fig. 2a, a design which was based on that of Land et al. (2001). The first stage consists of a precision instrumentation amplifier (Burr-Brown INA121, Digikey Inc.) in a differential configuration that provides very high input impedance (∼10^{12} ohms) and a gain of 10. The second stage is an ac-coupled amplifier (in active high pass configuration, with cutoff frequency 150 Hz) with gain 3.3, and comprises one-half of an LT1078 op-amp (Digikey, Inc.). The final stage has a gain of 33, and utilizes the other half of the LT1078. Both of these stages are inverting, resulting in a non-inverted output. The total gain of the completed amplifier was measured to be ∼1048. The bandwidth of the amplifier is limited by the final stage, and as the LT1078 has a gain-bandwidth product of 200 kHz, this limit is 6 kHz. With the amplifier inside a Faraday cage, the inputs referred noise level was measured to be 1.2 μV using a digital oscilloscope.

2.4. Cockroach coxa preparation

The flexible multielectrodes were fed into the cockroach coxa such that its recording sites were spread across several muscles. A Death's Head cockroach *Blaberus discoidalis* was chilled in an ice bucket for 20 min, and then pinned down, ventral side up, to a Sylgard dish. An incision was made in the coxa at the curved point where the medial surface of the coxa bends laterally to become the ventral surface. This corner is roughly ventral-most in the preparation, and allowed the electrode to be fed into the

Fig. 3. Insertion of fMEAs into coxa. An opaque sham electrode illustrates the position of the fMEA, and can be seen through the cuticle, inside the coxa. Devices are sandwiched between the inside surface of the cuticle and muscles in the coxa. Active electrodes were inserted further, with the fMEA tip curving into the body cavity. Nearby coxal muscles are roughly aligned with the rostro-caudal axis of the animal, and thus their fibers extend perpendicularly across the electrode shank.

coxa, moving medio-laterally, inside the coxa with recording sites facing inward, held against the inner ventral surface of the coxa by the internal tissue. The incision was approximately 1 mm wide, made midway between the coxa-body joint and the trochanter, on the left rear leg. A dummy electrode, opaque as to be visible through the cuticle, is seen in the preparation in Fig. 3. For the recordings presented in this paper, the multielectrode was positioned as seen in Fig. 3, but inserted to greater depth, where the expanding base of the electrode was flush with the incision in the cuticle.

2.5. Spike sorting

Spike waveforms were identified and extracted manually, using custom scripts written in Matlab (MathWorks, Inc.). The raw data were examined and all occurrences of clearly identifiable, unique spike waveforms were noted. A typical example of the spike waveform from each putative unit, $w(t)$, of time δT, was extracted and used to find similar waveforms from the raw multichannel data $s(t)$. For each channel, a filter output was computed from

$$f(t) = \int_0^{\delta T} (s(t+\tau) - w(\tau))^2 \, \mathrm{d}\tau$$

The sum of the filter outputs for each channel was used to detect individual multichannel spikes in the raw multichannel data.

3. Results

In initial experiments, attempts to insert the bare fMEAs into the coxa failed as the devices proved too compliant to be fed into the coxa. We mounted the devices on a semi-rigid plastic backing (3M Corp., Post-it #34-8506-7082-8), which provided the stiffness necessary to push past soft tissue whilst still conforming to more dense anatomical structures.

Upon insertion of the multielectrode array, motor and neural activity inside the coxa was observed on various subsets of the fMEA channels (Figs. 4 and 6). The activity consisted of units having a wide range of amplitudes and distributions across channels. Some smaller units such as that numbered 1 in Figs. 4 and 5 appeared on only one channel, whereas other smaller units (not shown) appeared across several channels. Whether these smaller units correspond to neural or muscular activity is difficult to determine, though the fast time course (<1 ms) of the positive phase of spike 1 (see positive peak in spike 1 on channel 6 in Fig. 5) could suggest single neural unit origin. Larger waveforms typically appeared in bursts during large thrashing movements of the leg (Figs. 4 and 6). These waveforms are most likely recordings of muscle activity. Qualitatively, each multielectrode captured two types of large waveform burst activity. The first type appeared mostly on the proximal recording sites of the multielectrode and second appeared on more distal sites. Based

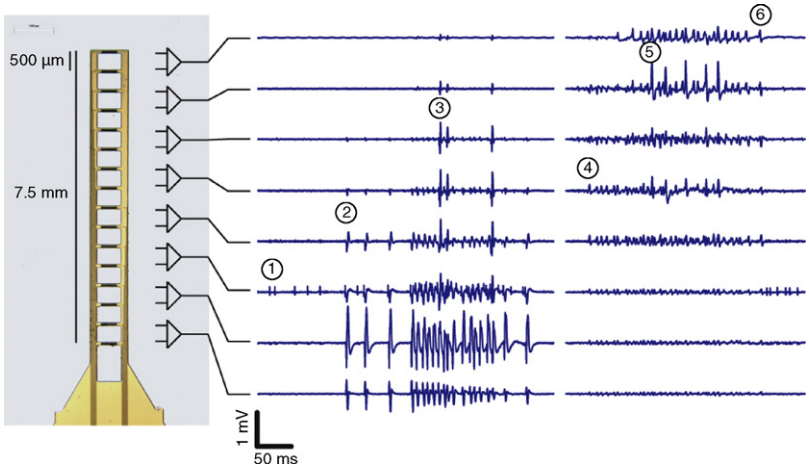

Fig. 4. Polyimide fMEA recording. Two bursts of raw multichannel data (right) recorded with the 16 recording site polyimide fMEA (left), during thrashing movements of the cockroach leg. Recording sites are oriented sequentially along the shank (left). Pairs of sites were connected to the differential amplifier in a bipolar recording configuration, utilizing the first eight channels. Six types of multichannel spike waveform were identified (right).

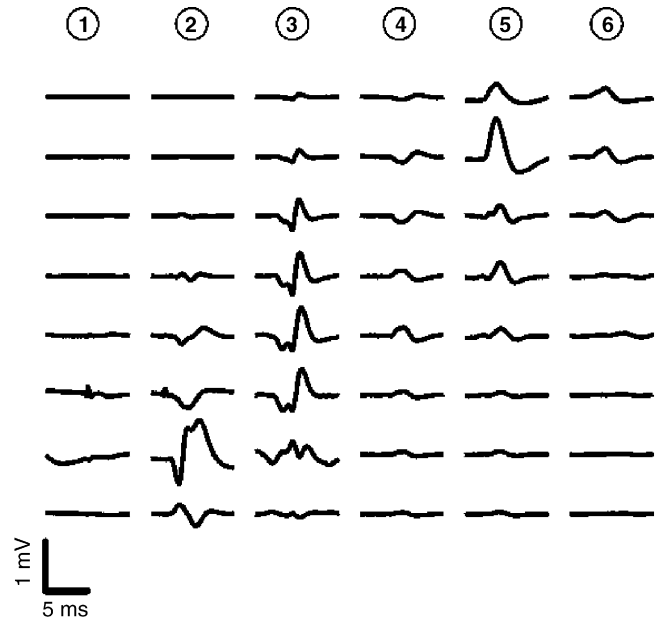

Fig. 5. Results of extraction and averaging of the multichannel spikes recorded with the polyimide fMEA. Labels (1–6) correspond to those in Fig. 4. Small (1, 4, and 6) and large (2, 3, and 5) amplitude spike waveforms appear, with varied spread (cf. 1 and 6 vs. 2–5) across channels. Spike 1 fired tonically, had smaller amplitude, and was localized to channel 6, whereas large spikes 2, 3, and 5 appeared only during strong thrashing bursts, and are highly likely to have muscular origin.

on the geometry of the preparation, the first type most likely corresponds to activity of femoral extensor muscles, whereas the second type corresponds to muscles nearer the body-coxa joint, most likely flexor or levator muscles (see Section 4).

Where individual units could be identified, a single clean example of the spike waveform was extracted (from all channels). This single multichannel spike was input to the filter described in Section 2.5, and the filter output thresholded to find other occurrences of the spike in a single 30 s recording. The extracted spikes were averaged to produce the spike templates seen in Figs. 5 and 7. Units 1–3 from the ladder array (Fig. 5) correspond to neural and muscle activity from tissues near the mid-ventral surface of the coxa. Units 4–6 are further dorsal and lateral in the coxa cavity, and correspond to activity picked up near the end of the array.

The bellows interconnect enabled bolt-on use of the fMEAs, greatly improving turn-around time when compared to wire-bonded interconnect solutions. An M3 bolt was fed through a rigid backing plate (in this case chips of the interconnect region of the fMEA that had previously been fabricated in silicon) and the multielectrode, and then screwed into the tapped hole in the Kel-F rod. The backing plate then uniformly compresses the fMEA interconnect pads onto the gold bellows.

To determine whether there were adverse affects of the fMEA on the animal's locomotion, a sham electrode consisting solely of the plastic backing material cut to the dimensions of the fMEA was fully inserted into the coxa, and high speed (500 frames/s) video taken of the animal running on a treadmill. Observers were unable to determine which of the hind legs of contained the implanted device, and the kinematics of hind leg motion appeared identical to that seen in normal running.

4. Discussion

The two flexible multielectrode arrays (fMEAs) and accompanying interface instrumentation we present can, upon insertion through a single slit in the surface of insect cuticle, record the activity of several distinct neuromuscular units. The resultant signals show strong isolation of units to small groups or individual fMEA channels. Their flexible nature allows them to bend around the inside of an insect appendage, accessing anatomically separate muscle groups. Preliminary high speed video studies of

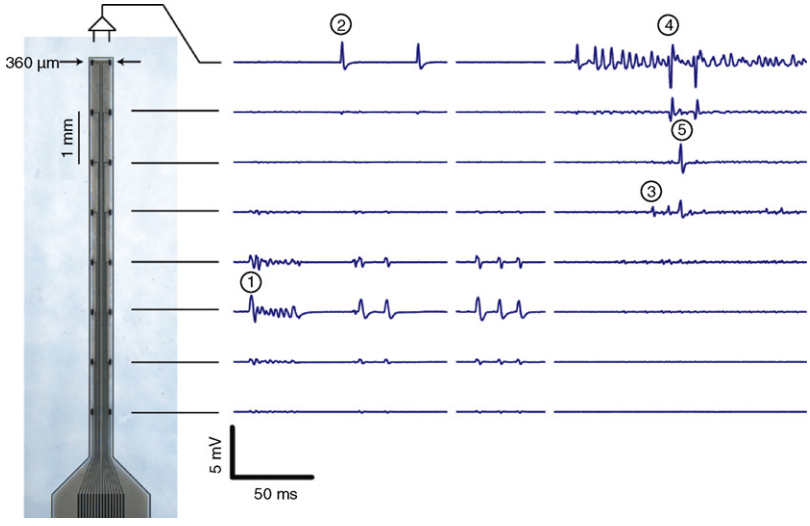

Fig. 6. Parylene fMEA recording. Three sections of raw multichannel data taken from two bursts of activity (right) recorded with the 16 recording site Parylene C fMEA (left), during thrashing movements of the cockroach leg. Recording sites are placed in eight pairs along the shank, with each pair having one site on either edge of the fMEA shank, spaced 360 µm apart (left). In this way, pairs of recording sites are roughly aligned parallel to muscle fibers in the cockroach coxa when the fMEA is inserted as seen in Fig. 3 Five types of multichannel spike waveform were identified (right). Noting the different scale bar here versus Fig. 4 (5 mV against 1 mV), the spikes are significantly larger in amplitude, and are spread across fewer channels.

animals running with an implanted sham electrode suggest that the inserted device does not affect the kinematics of the animal's locomotion. These results suggest fMEAs may offer a solution to gathering multiunit information from parts of the neuromuscular systems of behaving insects.

Adjusting the geometry of the recording sites of the fMEA to better match the anatomy of the muscles in the cockroach coxa gave recordings with better signal to noise ratio and channel separation (cf. Figs. 4–7, spike peak amplitudes and distribution across channels). Initial recordings made with fMEAs whose pairs of recording sites were oriented roughly perpendicular to the muscles (Fig. 4) yielded spikes with smaller peak amplitude, and that were typically distributed across several channels. Revised fMEAs with recording sites oriented parallel (Fig. 6) to the muscles produced larger peak amplitude spikes that were well isolated. While this result is expected from volume conductor theory (Trayanova et al., 1990), since aligning recording sites with active fibers increases the measured voltage difference, the effect is surprisingly strong given the anisotropy and heterogeneity of the tissues surrounding the device. Shunting effects of (conductive) hemolymph spreading across pairs of recording sites were apparently minimal, and were either mitigated by the large amplitude of the muscle spikes, or reduced by compression of the recording sites against the tissue by placing the device between the cuticle and musculature.

Adopting the naming convention of Carbonell (1947), as we proceed from the base of the fMEA to the tip, the device is first resting against muscles 179, then 180, and then encounters the muscle group 181, consisting of muscles 181a, 181b, and 181c as it traverses the ventral surface of the coxa. Further studies are needed to quantify the exact position of the array, but assuming that it continues to follow the curvature of the inner coxal cuticular surface, it next moves past muscle group 182 before encountering deeper body-coxal muscles. Muscle group 177 (the main extensor muscle group) and 178 (a posterior extensor muscle group), though not likely to be directly contacting the array, are located medially within the coxa, and hence are closer to the basal recording sites. Muscle 180 is an anterior flexor of the leg, 181 the main flexor, and 182 a second anterior flexor. Thus, qualitatively, the large spikes appearing near the base of the array (spikes 2 and 3 in Figs. 4 and 5, and spike 1 in Figs. 6 and 7) are most likely due to extensor muscles such as 177, 178, and 179. Spikes in the latter bursts appearing at the distal end of the array (spikes 5 and 6 in Figs. 4 and 5, and spikes 2, 4, and 5 in Figs. 6 and 7) most likely arise in the flexor muscles and muscle groups 180, 181, and 182.

A potential limitation of this technique lies in the variation of spike shape during appendage movement. The burst of spikes that potentially all arise from unit two in Fig. 4 and those of unit one in Fig. 6 have large variations in amplitude. How much of this variation lies in changes of spike shape due to bursting of the active fiber, and how much is due to movement of the recording sites relative to the fiber, is difficult to evaluate. This problem may be alleviated by anchoring the fMEA to the external cuticle, or by the increasingly sophisticated spike sorting methods that are becoming available for tracking changes in spike shape due to bursts (Penev et al., 2001).

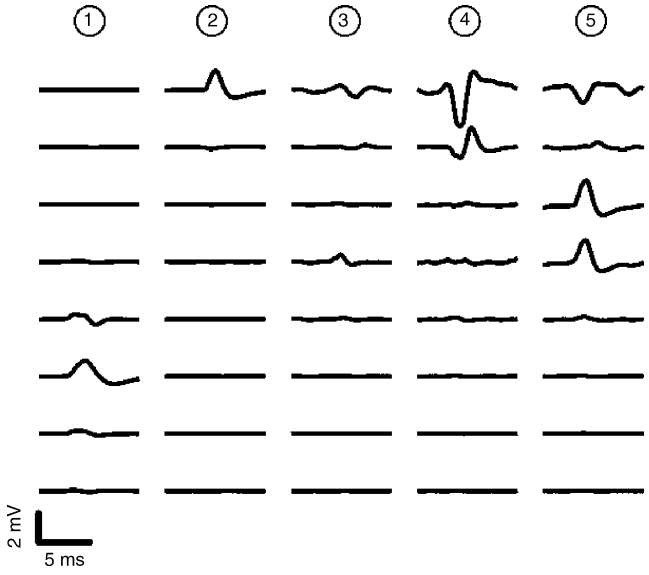

Fig. 7. Parylene fMEA averaged spike waveforms. Labels (1–5) correspond to those in Fig. 6. Spike 3 is the only unit of potentially neural origin. All spikes show improved channel separation (cf. Fig. 5), with spike 2 appearing only on channel 1, and others contained to small subsets of the fMEA recording sites.

The fMEAs we describe here would be suitable for chronic recording, having biocompatibility that should be identical or very similar to the polymer MEAs used by Lago et al. (2005) to record from the rat sciatic nerve for periods up to 12 months. In vertebrates, the success of long-term recording can be largely dependent on the type of preparation, and the degree to which encapsulation of the device by the immune response can be systematically avoided or reduced (Navarro et al., 2005). Their performance in long-term recordings from invertebrates will be the subject of future investigation. Devices which are not damaged during implantation or extraction can be cleaned in an ultrasonic organic solvent bath, and re-used.

The polyimide array recording sites have dimensions of $40\,\mu m \times 400\,\mu m$, and thus an area of $16{,}000\,\mu m^2$, while those on the parylene array are $40\,\mu m \times 100\,\mu m$, for an area of $4000\,\mu m^2$. These relatively large recording site areas ensure coupling capacitances that will be large enough for stimulation of tissue, either for functional electrophysiological and behavioral experiments, or for marking of tissue for localization of the fMEA post-experimentation. The electrode-electrolyte capacitance could be further increased by electroplating the recording sites (James et al., 2004). Through electromagnetic symmetry, the strong channel separation of units recorded with the fMEA implies that stimulation through the same pairs of fMEA sites will be strongly selective for individual units. This could provide a highly effective interface for functional electrical stimulation of multiple units (Kralj and Bajd, 1989).

Our novel interconnect allows acute manipulation of the device in a standard manipulator rod form factor, and provides simple bolt-on use and replacement of the fMEAs, eliminating the need for time consuming wire-bonding of each interconnect pad on each device. In addition, we have utilized surface-mount electronic components to design and build a compact 16 channel extracellular amplifier. The amplifier offers several advantages:

(1) small size that allows it to be placed inside a faraday cage, minimizing noise, (2) interconnection accomplished with a single cable plugged directly into the data acquisition board, (3) minimal cost, ∼$350 in components and circuit boards, and (4) portability. As the amplifier is 9 V battery powered, it may be used for field data acquisition experiments with multi-electrode arrays.

Future work will focus on identifying nerves and muscles responsible for each multichannel spike, improving the recording site geometry and electrode placement, and further miniaturization of the interconnect such that it may be attached to a freely behaving animal. At a thickness of ∼17 μm, the current devices are relatively thin. Future versions will be fabricated with a thick (tens to hundreds of μm) base layer, bringing the stiffness up to match that achieved with our plastic backing, and thus making the standalone devices suitable for implantantion.

Acknowledgements

The authors would like to thank all the members of the Isaacson, Hoy, Craighead, and Poly-PEDAL laboratories for their aid, as well as the staff and users of the Cornell Nanofabrication Facility. Dr. Conrad James and Marc Meyer for their aid in fabrication. Professor Robert Full, Shai Revzen, and the members of the Poly-PEDAL lab for their aid and input. This work supported by the W.M. Keck Foundation grant to establish a program in Nanobiotechnology at Cornell University, and a W.M. Keck Foundation Fellowship to A. Spence.

The Cornell Nanofabrication Facility is a member of the National Nanofabrication Users Network, and is funded by the National Science Foundation under Grant ECS-9731293, its users, Cornell University and Industrial Affiliates.

References

Ahn AN, Full RJ. A motor and a brake: two leg extensor muscles acting at the same joint manage energy differently in a running insect. J Exp Biol 2002;205(3):379–89.

Ando N, Shimoyama I, Kanzaki R. A dual-channel fm transmitter for acquisition of flight muscle activities from the freely flying hawkmoth, agrius convolvuli. J Neurosci Meth 2002;115(2):181–7.

Bassler U. The femur-tibia control-system of stick insects—a model system for the study of the neural basis of joint control. Brain Res Rev 1993;18(2):207–26.

Bassler U, Buschges A. Pattern generation for stick insect walking movements—multisensory control of a locomotor program. Brain Res Rev 1998;27(1):65–88.

Berdondini L, Chiappalone M, van der Wal P, Imfeld K, de Rooij N, Koudelka-Hep M, et al. A microelectrode array (mea) integrated with clustering structures for investigating in vitro neurodynamics in confined interconnected sub-populations of neurons. Sens Actuators B: Chem 2006;114(1):530–41.

Carbonell C. The thoracic muscles of the cockroach *Periplaneta americana* (l.). Smithson Misc Collect 1947;107(2):1–23.

Christensen TA, Pawlowski VM, Lei H, Hildebrand JG. Multi-unit recordings reveal context-dependent modulation of synchrony in odor-specific neural ensembles. Nat Neurosci 2000;3(9):927–31.

Deliagina TG, Zelenin PV, Fagerstedt P, Grillner S, Orlovsky GN. Activity of reticulospinal neurons during locomotion in the freely behaving lamprey. J Neurophysiol 2000;83(2):853–63.

Durr V, Schmitz J, Cruse H. Behaviour-based modelling of hexapod locomotion: linking biology and technical application. Arthropod Struct Dev 2004;33(3):237–50.

Frye MA, Olberg RM. Visual receptive-field properties of feature detecting neurons in the dragonfly. J Comp Physiol a-Sens Neural Behav Physiol 1995;177(5):569–76.

Full RJ, Koditschek DE. Templates and anchors: neuromechanical hypotheses of legged locomotion on land. J Exp Biol 1999;202(23):3325–32.

Ghigliazza RM, Holmes P. A minimal model of a central pattern generator and motoneurons for insect locomotion. Siam J Appl Dyn Syst 2004;3(4):671–700.

Ghigliazza RM, Holmes P. Towards a neuromechanical model for insect locomotion: hybrid dynamical systems. Regular Chaotic Dyn 2005;10(2):193–225.

Ghigliazza RM, Altendorfer R, Holmes P, Koditschek D. A simply stabilized running model. Siam J Appl Dyn Syst 2003;2(2):187–218.

Gregor RJ, Smith DW, Prilutsky BI. Mechanics of slope walking in the cat: quantification of muscle load, length change, and ankle extensor emg patterns. J Neurophysiol 2006;95(3):1397–409.

Gronenberg W. The fast mandible strike in the trap-jaw ant odontomachus. 1. Temporal properties and morphological-characteristics. J Comp Physiol a-Sens Neural Behav Physiol 1995a;176(3):391–8.

Gronenberg W. The fast mandible strike in the trap-jaw ant odon-tomachus. 2. Motor control. J Comp Physiol a-Sens Neural Behav Physiol 1995b;176(3):399–408.

Higham TE, Jayne BC. In vivo muscle activity in the hindlimb of the arboreal lizard, chamaeleo calyptratus: general patterns and the effects of incline. J Exp Biol 2004;207(2):249–61.

Holmes P, Full RJ, Koditschek D, Guckenheimer J. The dynamics of legged locomotion: Models, analyses, and challenges. Siam Rev 2006;48(2):207–304.

James CD, Spence AJH, Dowell N, Hussein RJ, Smith K, Craighead HG, et al. Extracellular recordings from constructed neuronal networks using planar microelectrode arrays. IEEE Trans Biomed Eng 2004;51(9):1640–8.

Koditschek DE, Full RJ, Buehler M. Mechanical aspects of legged locomotion control. Arthropod Struct Dev 2004;33(3):251–72.

Kralj A, Bajd T. Functional electrical stimulation: standing and walking after spinal cord injury. Boca Raton, FL: CRC Press Inc; 1989.

Kutsch W. Transmission of muscle potentials during free flight of locusts. Comput Electron Agric 2002;35(2–3):181–99.

Lago N, Ceballos D, Rodriguez FJ, Stieglitz T, Navarro X. Long term assessment of axonal regeneration through polyimide regenerative electrodes to interface the peripheral nerve. Biomaterials 2005;26(14):2021–31.

Land BR, Wyttenbach RA, Johnson BR. Tools for physiology labs: an inexpensive high-performance amplifier and electrode for extracellular recording. J Neurosci Meth 2001;106(1):47–55.

Lapatki BG, van Dijk JP, Jonas IE, Zwarts MJ, Stegeman DF. A thin, flexible multielectrode grid for high-density surface emg. J Appl Physiol 2004;96(1):327–36.

Lehmkuhle MJ, Normann RA, Maynard EM. Trial-by-trial discrimination of three enantiomer pairs by neural ensembles in mammalian olfactory bulb. J Neurophysiol 2006;95(3):1369–79.

Leutgeb S, Letugeb JK, Barnes CA, Moser EI, McNaughton BL, Moser MB. Independent codes for spatial and episodic memory in hippocampal neuronal ensembles. Science 2005;309(5734):619–23.

Marder E, Calabrese RL. Principles of rhythmic motor pattern generation. Physiol Rev 1996;76(3):687–717.

Margalit E, et al. Retinal prosthesis for the blind. Survey of ophthalmology 2002;47(4):335–56.

Mu LY, Ritzmann RE. Kinematics and motor activity during tethered walking and turning in the cockroach, *Blaberus discoidalis*. J Comp Physiol a-Neuroethol Sens Neural Behav Physiol 2005;191(11):1037–54.

Murphy, D., 2003. Flexible polyimide based microfluidic and microelectronic neural probes. Masters thesis, Cornell University.

Navarro X, Krueger TB, Lago N, Micera S, Stieglitz T, Dario P. A critical review of interfaces with the peripheral nervous system for the control of neuroprostheses and hybrid bionic systems. J Peripheral Nervous Syst 2005;10(3):229–58.

Pearson KG, Wong RKS, Fourtner CR. Connections between hair-plate afferents and motoneurons in cockroach leg. J Exp Biol 1976;64(1):251–66.

Penev PS, Dimitrov AG, Miller JP. Characterization of and compensation for the nonstationarity of spike shapes during physiological recordings. Neurocomputing 2001;38–40:1695–701.

Quimby LA, Amer AS, Zill SN. Common motor mechanisms support body load in serially homologous legs of cockroaches in posture and walking. J Comp Physiol a-Neuroethol Sens Neural Behav Physiol 2006;192(3):247–66.

Rodger D, Li W, Guven D, Weiland J, Humayun M, Tai YC. Flexible parylene multielectrode system for the intraocular retinal prosthesis. Invest Ophthalmol Visual Sci 2005;46(Supplement S46).

Rodriguez FJ, Ceballos D, Schuttler M, Valero A, Valderrama E, Stieglitz T, et al. Polyimide cuff electrodes for peripheral nerve stimulation. J Neurosci Meth 2000;98(2):105–18.

Seipel JE, Holmes PJ, Full RJ. Dynamics and stability of insect locomotion: a hexapedal model for horizontal plane motions. Biol Cybernetics 2004;91(2):76–90.

Smirnakis SM, Berry MJ, Warland DK, Bialek W, Meister M. Adaptation of retinal processing to image contrast and spatial scale. Nature 1997;386(6620):69–73.

Stieglitz T, Gross M. Flexible biomems with electrode arrangements on front and back side as key component in neural prostheses and biohybrid systems. Sens Actuators B-Chem 2002;83(1–3):8–14.

Stieglitz T, Schuettler M, Schneider A, Valderrama E, Navarro X. Noninvasive measurement of torque development in the rat foot: measurement setup and results from stimulation of the sciatic nerve with polyimide-based cuff electrodes. IEEE Trans Neural Syst Rehabil Eng 2003;11(4):427–37.

Takeuchi S, Shimoyama I. A radio-telemetry system with a shape memory alloy microelectrode for neural recording of freely moving insects. Biomed Eng, IEEE Trans 2004;51(1):133–7.

Theunissen F, Roddey JC, Stufflebeam S, Clague H, Miller JP. Information theoretic analysis of dynamical encoding by four identified primary sensory interneurons in the cricket cercal system. J Neurophysiol 1996;75(4):1345–64.

Trayanova N, Henriquez CS, Plonsey R. Extracellular potentials and currents of a single active fiber in a restricted volume conductor. Ann Biomed Eng 1990;18(3):219–38.

Weimann JM, Skiebe P, Heinzel H-G, Soto C, Kopell N, Jorge-Rivera JC, et al. Modulation of oscillator interactions in the crab stomatogastric ganglion by crustacean cardioactive peptide. J Neurosci 1997;17(5):1748–60.

Winters JM, Woo SLY. Winters JM, Woo SL-Y, editors. Multiple muscle systems/biomechanics and movement organization. New York: Springer-Verlag; 1990.

Wise KD. Silicon microsystems for neuroscience and neural prostheses. IEEE Eng Med Biol Mag 2005;24(5):22–9.